

Modeling state-transition dynamics in brain signals by memoryless Gaussian mixtures

Takahiro Ezaki,^{1,2} Yu Himeno,³ Takamitsu Watanabe,^{4,5} and Naoki Masuda^{6,7,*}

¹*Research Center for Advanced Science and Technology,
The University of Tokyo, 4-6-1 Komaba, Meguro-ku, Tokyo 153-8904, Japan*

²*PRESTO, JST, 4-1-8 Honcho, Kawaguchi, Saitama 332-0012, Japan*

³*Department of Aeronautics and Astronautics, The University of Tokyo,
7-3-1 Hongo, Bunkyo-ku, Tokyo 113-8656, Japan*

⁴*Laboratory for Cognition Circuit Dynamics,
RIKEN Centre for Brain Science, Saitama 351-0198, Japan*

⁵*International Research Center for Neurointelligence,
The University of Tokyo 7-3-1 Hongo Bunkyo-ku, Tokyo 113-0033 Japan*

⁶*Department of Mathematics, State University of
New York at Buffalo, Buffalo, NY 14260-2900, USA*

⁷*Computational and Data-Enabled Science and Engineering Program,
State University of New York at Buffalo, Buffalo, NY 14260-5030, USA*

Abstract

Recent studies have proposed that one can summarize brain activity into dynamics among a relatively small number of hidden states and that such an approach is a promising tool for revealing brain function. Hidden Markov models (HMMs) are a prevalent approach to inferring such neural dynamics among discrete brain states. However, the validity of modeling neural time series data with HMMs has not been established. Here, to address this situation and examine the performance of the HMM, we compare the model with the Gaussian mixture model (GMM), which is a statistically simpler model than the HMM with no assumption of Markovianity, by applying both models to synthetic and empirical resting-state functional magnetic resonance imaging (fMRI) data. We find that the GMM allows us to interpret the sequence of the estimated hidden states as a time series obeying some patterns and is often better than HMMs in terms of the accuracy and consistency of estimating the time course of the hidden state. These results suggest that GMMs can be a model of first choice for investigating hidden-state dynamics in data even if the time series is apparently not memoryless.

* naokimas@buffalo.edu

I. INTRODUCTION

Brain dynamics are a product of large-scale networks realized by interaction of functionally specialized regions in the brain [1–4]. Such dynamics have been considered to underpin the integration of information [5], cognitive functions [6], and their impairments (i.e., neuropsychiatric disorders) [7]. Understanding dynamical coordination of brain regions necessitates data-analysis methods that reduce the dimension of large-scale neural data, which are often provided in the form of multivariate time series, without losing much information. Widely used examples include independent component analysis [8] and network analysis [3, 9].

One approach to investigating integrated dynamics of multivariate time-varying neural signals is to assume a relatively small number of latent states and summarize the multidimensional brain activity data at each time point into one of these states. One can estimate time series of the latent state by, for example, the hidden Markov models (HMMs) [10–18], dynamic functional connectivity [19, 20], and energy landscape analysis [21–23]. This strategy allows us to continue to work on the same time domain as the original data, and therefore to, e.g., compute transition rates between the latent states and interpret state transition events, rather than to reduce the data to static measures (e.g., functional connectivity) or transform the data to the frequency domain implicitly assuming stationarity of the time series. State-transition dynamics have been reported to be closely related to various functions of the brain, including executive function [24], decision-making [25], and to psychiatric conditions such as autism [26] and schizophrenia [27]. For example, Ezaki et al. [24] analyzed resting-state functional magnetic resonance imaging (fMRI) data obtained from healthy humans using the energy landscape analysis. They showed that the ease of state transitions between synchronized activity patterns of specific regions of interest (ROIs) explained age-related changes in executive functions. Taghia et al. [25] applied a Bayesian switching linear dynamical systems model to fMRI data obtained from participants performing a n -back working memory task. They found a task-specific hidden state and dynamical switching path of the estimated hidden states. Using the energy landscape analysis, Watanabe et al. [26] showed that high functioning autistic adults had atypically stable brain dynamics with lower transition rates among different brain systems and longer dwelling time, and that such over-stability was predictive of both their symptom severity and unique cognitive skills. For resting-state fMRI data obtained from individuals with schizophrenia, Kottaram et al. [27] reported aberrant transition dynamics among latent states estimated by an HMM. Relevance of hidden states to task-related data in a supervised set-

ting has also been reported. Vidaurre et al. [17] found hidden states representing task-related brain states using magnetoencephalography (MEG) data during a button press task.

Among these methods, the HMMs have been widely used for studying fMRI [11, 14, 15, 17] and MEG [10, 12, 13, 16–18] data recorded from the human brain. The HMM is a model comprising a set of probability distributions of the observables each of which corresponds to a latent (hidden) state and the transition probabilities between the pairs of latent states. By assumption, the state-transition dynamics of an HMM are Markovian, i.e., with no memory effect longer than a single time step. HMMs have been useful in modeling neural dynamics for the following reasons. First, they can be applied to relatively high-dimensional time series [10, 16–18]. Second, they can detect changes in signals without delay in the form of changes in the latent state, which is not straightforward with dynamic functional connectivity calculated with sliding time windows [18].

The HMM modeling is based on the implicit assumption that the stochastic rule of state transitions depends on the last state and not on the states in the further past, i.e., Markovian property. In fact, the validity of this assumption has not been thoroughly validated at least for fMRI data. The potential lack of Markovianity may be detrimental to the HMM modeling.

The same analysis pipeline to infer hidden states of the time series data (Fig. 1) can be realized by a simple static mixture model that does not assume such Markovianity. Mixture models have been used in neuroimaging research for detecting activation of brain regions [28, 29] and clustering them into larger ROIs [30]. In Refs. [28, 29], for example, a mixture model with two probability distributions corresponding to activation and deactivation of each voxel, respectively, was used to classify the state of the voxels. However, to the best of our knowledge, mixture models have not been used for studying dynamical state transitions in neuroimaging data. Because mixture models do not assume any temporal structure, they are not influenced by the sampling rate and therefore may serve as useful baseline models with which to assess the validity of fitting HMMs. If state transitions in the given data are considerably influenced by the previous state but not the states in the further past, an HMM is expected to perform better than a mixture model. In contrast, if state transitions either do not depend on any past states or do depend on the history of the state earlier than the last state, mixture models may outperform HMMs because of their relative simplicity. In general, complex models may overfit to the data, and their model estimation algorithms are often computationally costly and may end up converging to local optima.

Therefore, to examine the validity of Markovianity in the HMM, we compare the HMM and Gaussian mixture model (GMM), a mixture model. The GMM was chosen because, in HMMs

applied to neuroimaging data, the Gaussian distribution is widely used as the probability distribution conditioned on the hidden state [10–18]. Then, if we ignore state-transition dynamics as described by a hidden Markov process, the distribution of signals as estimated by the fitting of an HMM is a GMM. Therefore, in the present study, we compare HMMs and GMMs in terms of (i) accuracy of fit to synthetic time series for which true hidden states are known and (ii) robustness of the estimated hidden states for resting-state fMRI data across different experimental sessions. We show that GMMs often outperform HMMs for synthetic and empirical data in terms of the accuracy and robustness of estimating time courses of the hidden state. On that basis, we propose mixture models as another promising alternative when we test hypotheses involving dynamics of hidden states in fMRI and potentially other types of data.

II. MATERIALS AND METHODS

An overview of the analysis pipeline is shown in Fig. 1.

A. Gaussian Mixture model

Assume that there are t_{\max} observations of N dimensional data, \mathbf{x}_t ($t = 1, \dots, t_{\max}$) (Fig. 1(a)). Our Gaussian mixture model assumes that each observation, \mathbf{x}_t , is generated from one of the two Gaussian distributions (Fig. 1(b)). We set the number of states to two for simplicity. The probability density of the observed data conditioned on the state is given by $\mathcal{N}(\boldsymbol{\mu}_{s_t}, \boldsymbol{\Sigma}_{s_t})$, where $s_t \in \{1, 2\}$ is the hidden (i.e., latent) state, \mathcal{N} denotes a N -dimensional multivariate Gaussian distribution, and $\boldsymbol{\mu}_{s_t}$ and $\boldsymbol{\Sigma}_{s_t}$ are the mean and covariance matrix of the Gaussian distribution under hidden state s_t , respectively. The marginal probability distribution of \mathbf{x}_t is given by

$$P(\mathbf{x}_t) = \sum_{s=1}^2 \pi_s \mathcal{N}(\mathbf{x}_t | \boldsymbol{\mu}_s, \boldsymbol{\Sigma}_s), \quad (1)$$

where π_s is the probability that hidden state s is taken. One estimates π_s , $\boldsymbol{\mu}_s$, and $\boldsymbol{\Sigma}_s$ ($s = 1, 2$) by maximizing the log-likelihood function given by

$$\ln P(\mathbf{x}_1, \mathbf{x}_2, \dots, \mathbf{x}_{t_{\max}} | \boldsymbol{\pi}, \boldsymbol{\mu}, \boldsymbol{\Sigma}) = \sum_{t=1}^{t_{\max}} \ln \left\{ \sum_{s=1}^2 \pi_s \mathcal{N}(\mathbf{x}_t | \boldsymbol{\mu}_s, \boldsymbol{\Sigma}_s) \right\}. \quad (2)$$

We used the expectation-maximization (EM) algorithm, which is typically used for maximizing Eq. (2) [31, 32].

Then, the time course of the hidden state, \hat{s}_t ($t = 1, \dots, t_{\max}$), given the observations is estimated by

$$\hat{s}_t = \arg \max_s P(s|\mathbf{x}_t) = \arg \max_s \frac{\hat{\pi}_s \mathcal{N}(\mathbf{x}_t | \hat{\boldsymbol{\mu}}_s, \hat{\boldsymbol{\Sigma}}_s)}{\sum_{r=1}^2 \hat{\pi}_r \mathcal{N}(\mathbf{x}_t | \hat{\boldsymbol{\mu}}_r, \hat{\boldsymbol{\Sigma}}_r)}, \quad (3)$$

where $\hat{\pi}_s$, $\hat{\boldsymbol{\mu}}_s$, and $\hat{\boldsymbol{\Sigma}}_s$ are the maximum likelihood estimator obtained by the EM algorithm.

We analyze the data using the GMM package in *scikit-learn* [33]. We used the default setting of *scikit-learn* for determining the initial conditions for the EM algorithm.

B. Hidden Markov model

We consider HMMs with Gaussian components [34] (Fig. 1(c)). The model assumes that each of the N -dimensional observations \mathbf{x}_t ($t = 1, \dots, t_{\max}$) is generated from one of the two Gaussian distributions, as in GMMs, and that s_t ($t = 1, \dots, t_{\max}$) obeys first-order Markovian dynamics given by

$$P(s_t | s_1, \dots, s_{t-1}) = P(s_t | s_{t-1}). \quad (4)$$

To estimate the HMM, we used an EM algorithm known as the Baum-Welch algorithm [35]. We used the Viterbi algorithm [36] to estimate the time course of the hidden state given the observations. We estimated HMMs for our data using a python package *hmmlearn* (<https://hmmlearn.readthedocs.io/>), which was originally developed as part of *scikit-learn* [32]. We used the default setting of *hmmlearn* for determining the initial conditions for the EM algorithm. We confirmed that the variational Bayes (VB) algorithm for estimating the HMM, which is also widely used [37], yielded qualitatively similar results to those obtained by the EM algorithm (Supporting Information, Fig. S1).

The EM algorithm does not guarantee the exact optimization due to local minima. Therefore, for both GMM and HMM, we carried out the optimization procedure 10 times and adopted the model that attained the largest likelihood. In the present study, all the estimations successfully converged.

C. Synthetic data

To compare the performance between the GMM and HMM, we generated six types of synthetic time series of $N = 50$ dimensions, modeling fMRI signals recorded from 50 ROIs.

In section II C 1, we explain the sum of the empirical fMRI signals and added global noise, denoted by \tilde{x}_t , for which we fit a mixture of two Gaussian distributions. In section II C 2, we explain how to fit a mixture of two Gaussian distributions to \tilde{x}_t and the procedure to generate x_t given the hidden state. In section II C 3, we explain dynamical rules with which to generate time series of the hidden state. As a combination of one of the three dynamical rules for the hidden state and either the presence or absence of the added global noise, we consider six types of synthetic time series, x_t .

1. Empirical fMRI signals with additional global noise

We set

$$\tilde{x}_t = \tilde{y}_t + \epsilon_t, \tag{5}$$

where \tilde{y}_t is the N -dimensional empirical fMRI signal at time (i.e., volume) t , and

$$\epsilon_t = c\xi_t \times (1, 1, \dots, 1) \tag{6}$$

is a global signal. In Eq. (6), ξ_t obeys a one-dimensional standard normal distribution (i.e, $\xi_t \sim \mathcal{N}(0, 1)$) that is independent for different t , and c is the magnitude of the added global signal. Global noise may be already present in the original fMRI data [38]. Global signal contains non-neural confounds, but it is also considered to reflect neural activity relevant to cognition and behavior [39]. In general, $\{\tilde{x}_t\}$ is more correlated between regions when the global signal is present than absent. Here we consider the additional global noise term to assess the performance of GMMs and HMMs in estimating state-transition dynamics under different amounts of correlation among ROIs. We use $c = 0$ and $c = 1$, which correspond to the absence and presence of the additional global signal, respectively.

2. Fitting of a mixture of two Gaussian distributions

A previous study reported that the hidden states of resting-state fMRI data were clustered into two macroscopic states [14]. Therefore, we assume that $\tilde{\mathbf{x}}_t$ obeys a state-dependent N -dimensional Gaussian distribution with two hidden states, $s_t \in \{1, 2\}$, i.e.,

$$\tilde{\mathbf{x}}_t \sim \begin{cases} \mathcal{N}(\boldsymbol{\mu}_1, \boldsymbol{\Sigma}_1), & \text{if } s_t = 1, \\ \mathcal{N}(\boldsymbol{\mu}_2, \boldsymbol{\Sigma}_2), & \text{if } s_t = 2. \end{cases} \quad (7)$$

We set the parameters of the two Gaussian distributions (i.e., $\boldsymbol{\mu}_1$, $\boldsymbol{\Sigma}_1$, $\boldsymbol{\mu}_2$, and $\boldsymbol{\Sigma}_2$) as follows. First, resting-state fMRI data obtained from N ROIs, where we set $N = 50$ (see Sec. IID for details of the fMRI data) provide N -dimensional time series. Second, we concatenated the fMRI data recorded in all the sessions for a single participant into one N -dimensional time series and then concatenated the time series for all the participants into one time series. Depending on the value of c (i.e., with and without the global noise), we computed $\tilde{\mathbf{x}}_t$ using Eqs. (5) and (6). Third, we fitted a GMM with two Gaussian components to the time series by maximum likelihood estimation. Fourth, we discarded the estimated mixture weights (i.e., π_1 and $\pi_2 = 1 - \pi_1$) such that we only used the parameter values of the two estimated Gaussian distributions.

After we estimated the two Gaussian distributions, we generated \mathbf{x}_t by first determining s_t according to the method described in section IIC 3 and then drawing \mathbf{x}_t according to the Gaussian distribution corresponding to s_t .

In one set of numerical simulations, we varied the means of the obtained Gaussian distributions as $\mathcal{N}(\alpha\boldsymbol{\mu}_i, \boldsymbol{\Sigma}_i)$ ($i = 1, 2$), where $\alpha (> 0)$ is a parameter controlling the difficulty of the estimation problem; the estimation of the hidden-state dynamics and the probability distribution of the observable is difficult when α is small.

3. Dynamics of the hidden state

We consider the following three rules governing the state transitions.

First, in the so-called *Bernoulli* dynamics, at each time point, one of the two hidden states was selected with the equal probability, i.e., 0.5, regardless of the states in the past.

Second, in the *deterministic dynamics*, the initial hidden state s_1 is equal to 1 or 2 with the equal probability, i.e., 0.5. We denote by \bar{s}_1 the state that is opposite to s_1 , i.e., $\bar{s}_1 = 3 - s_1$. The

hidden state was flipped every two time steps (“...11221122...”). Formally, for $1 < t \leq t_{\max}$, we set

$$s_t = \begin{cases} s_1 & (t = 4m + 1, 4m + 2), \\ \bar{s}_1 & (t = 4m + 3, 4m + 4), \end{cases} \quad (8)$$

where $m = 0, 1, 2, \dots$

Third, in the *Markov dynamics*, the initial hidden state s_1 was either 1 or 2 with the equal probability, i.e., 0.5. Then, the time course of the hidden state obeys a Markov chain, of which the state-transition probabilities are given by $P(s_t = 1|s_{t-1} = 1) = 0.948$, $P(s_t = 1|s_{t-1} = 2) = 0.052$, $P(s_t = 2|s_{t-1} = 1) = 0.044$, and $P(s_t = 2|s_{t-1} = 2) = 0.956$. We used these values because they were the values for the HMM fitted to the fMRI data in the case of $N = 50$ and $c = 0$.

D. fMRI data

We used extensively pre-processed fMRI data provided by the Human Connectome Project, S1200 Release (<https://www.humanconnectome.org/>) [40]. The data set includes time series for each component obtained by the independent component analysis (ICA) applied to fMRI signals recorded from 1,003 participants (22–35yo, 534 females). These participants completed four sessions of 15-min echo planar imaging (EPI) sequence on a 3T Siemens Connectome-Skyra (TR = 0.72 s, TE= 33.1 ms, 72 slices, 2.0 mm isotopic; FOV = 208 × 180 mm) and a single T1-weighted sequence (TR = 2.4 s, TE = 2.14 ms, 0.7 mm isotopic, FOV = 224 × 224 mm). Each session yielded 1,200 volumes (i.e., observations) of EPI images. The fMRI data were first minimally pre-processed according to Ref. [41]. Then, artifacts were removed using ICA+FIX [42, 43] and inter-participant registration of cerebral cortex using MSMAll [44, 45]. The preprocessed data then underwent a group principal component analysis (PCA) using MIGP [46]. The resulting eigenmap was fed to group-ICA, which was performed by FSL’s tool MELODIC [47, 48]. The group-ICA was carried out for dimensions (i.e., number of independent components) $N = 15, 25, 50, 100, 200$, and 300. We did not use group-ICA data generated with $N = 100, 200$, and 300 because of high computational cost for estimating the models used in the present study. In addition, we prepared data with $N = 5$ and 10 components by using the first 5 and 10 independent components in the $N = 15$ data set, respectively.

Unless we state otherwise in Sec. III C, we fed the fMRI data to algorithms for estimating

GMMs or HMMs after concatenating the observed signals obtained from all the sessions from a single participant into one sequence and then the sequences obtained from all the participants into one sequence. In the concatenated data, the final volume of sessions 1, 2, and 3 is followed by the first volume of sessions 2, 3, and 4, respectively, although different sessions are not causally related to each other. In practice, the influence of the concatenation on the estimation of the HMM is considered to be negligible because each session is sufficiently long (i.e., 1,200 volumes) [14, 18].

III. RESULTS

A. State-transition dynamics compared between the HMM and fMRI data

In contrast to GMMs, HMMs assume Markovian state dynamics, while the state dynamics inferred for the given empirical data may considerably deviate from Markovian dynamics. Therefore, we started by comparing the transition probabilities between hidden states 1 and 2 predicted by the estimated HMM (i.e., $P(s_t = 1|s_{t-1} = 2)$ and $P(s_t = 2|s_{t-1} = 1)$) and those directly calculated for the fMRI data. We calculated the state-transition probabilities for the fMRI data as follows. First, we estimated the HMM for the fMRI data concatenated over all sessions and participants. Second, we determined the hidden state at each time point in the concatenated time series as the one such that the likelihood conditioned on the state is larger than the likelihood conditioned on the other state. Third, we extracted the time series of the hidden state for each session and each individual. Fourth, for each session and participant, we defined the transition probability from state 1 to 2 conditioned on state 1 by $C(s_{t-1} = 1 \text{ and } s_t = 2) / [C(s_{t-1} = 1 \text{ and } s_t = 1) + C(s_{t-1} = 1 \text{ and } s_t = 2)]$, where $C(\cdot)$ denotes the count of the event in the argument over $2 \leq t \leq 1,200$. Similarly, the transition probability from state 2 to 1 conditioned on state 2 is given by $C(s_{t-1} = 2 \text{ and } s_t = 1) / [C(s_{t-1} = 2 \text{ and } s_t = 1) + C(s_{t-1} = 2 \text{ and } s_t = 2)]$. Finally, we averaged the results over all the sessions and participants.

We found that the transition probabilities implied by the estimated HMMs were substantially larger than those directly computed from the empirical transitions (by 18–34%; Table I). Therefore, for the present data set, the dynamics of the hidden state assumed by the HMM are not that close to the state dynamics directly observed for the data.

Using the estimated HMMs and the time courses of the hidden state for the fMRI data, we

also examined the duration of the hidden state. The duration of the hidden state is defined by the number of successive volumes for which the hidden state remains the same before it flips. Denote by d the duration of hidden state 1. The distribution of d directly calculated for the fMRI data is shown by the solid lines in Fig. 2. The distributions have a peak marking a typical time scale of the dynamics. In contrast, the HMM assumes a geometric distribution, $p_{11}^d(1 - p_{11})$, where $p_{11} = P(s_t = 1 | s_{t-1} = 1)$. The geometric distribution monotonically decreases in terms of d , as shown by the dashed lines in Fig. 2. The empirical distributions were significantly different from the geometric distribution (Kolmogorov-Smirnov test; $N = 5$: Kolmogorov-Smirnov statistic $D_{116722} = 0.21$; $N = 10$: $D_{111090} = 0.20$; $N = 15$: $D_{117709} = 0.20$; $N = 25$: $D_{109005} = 0.19$; $N = 50$: $D_{91166} = 0.13$; $p < 10^{-136}$ in all the cases). The discrepancy between the actual distribution of d given the hidden states estimated by the HMM and the distribution of d implied by the HMM indicates that the present fMRI data as multivariate time series may not be reasonably described by HMMs.

B. Accuracy of estimating the hidden states for synthetic time series

We then compared the accuracy of estimating the hidden states between the GMM and HMM using the synthetic time series, for which the true hidden states are known. The aim of this analysis is to show that the HMM is not always more accurate than the GMM. In particular, the GMM outperforms the HMM in some cases even if the time series was generated in a hidden Markovian manner.

We consider either the presence of the global signal (i.e., $c = 1$ in Eq. (6)) or its absence (i.e., $c = 0$). We also consider one of the three types of hidden-state dynamics, i.e., Bernoulli, deterministic, or Markov. We refer to a combination of these two factors as a condition; there are six conditions each of which generates a different type of N -dimensional synthetic time series. Under each condition, we generated synthetic time series of length $t_{\max} = 10^4$. We varied the means of Gaussian distributions through parameter α (see Methods). To each of the N -dimensional synthetic time series, we fitted the GMM and HMM and inferred the hidden state at each time point. The accuracy score was defined as the number of time points at which the hidden state was correctly estimated, which was then divided by t_{\max} . If the estimation is completely at random, the accuracy score is approximately equal to 0.5. For each α value and each of the six conditions, we generated 20 synthetic time series and computed the average and standard deviation of the

accuracy score. The results are shown in Fig. 3, where each panel corresponds to a condition. The figure indicates that the accuracy score is higher for the HMM than the GMM in some cases and vice versa in other cases.

C. Consistency in the estimation of the hidden state across different recording sessions

For the fMRI data, we cannot evaluate the accuracy of estimating the hidden state because the true hidden states are unknown. Therefore, we examined for each participant the extent to which the frequency of the estimated hidden states was conserved across resting-state recording sessions of the experiment. This analysis stands on the premise that, if hidden states characterize fMRI signals, their properties such as the frequency of each hidden state should be similar across different sessions, which is supported by a previous study [14].

First, for each dimension $N = 5, 10, 15, 25, 50$, we fitted the GMM and HMM with two components (equivalent to the hidden states) to the fMRI signals for each participant, which were the concatenation of the signals over four sessions each of which contained 1,200 volumes. Then, for each participant, we labeled the hidden state that appeared more frequently as state 1 and the other as state 2. We denote the frequency of the two states computed for each participant and session by $\tilde{\pi}_1^{(j)}$ and $\tilde{\pi}_2^{(j)} (= 1 - \tilde{\pi}_1^{(j)})$, respectively, where $j (= 1, 2, 3, 4)$ represents the session. To quantify how the frequency of the hidden states is consistent across sessions, we define the inconsistency score for each participant by $\sigma[\tilde{\pi}_1]/E[\tilde{\pi}_1]$, where $\sigma[\tilde{\pi}_1]$ and $E[\tilde{\pi}_1]$ are the standard deviation and the average of $\tilde{\pi}_1^{(j)}$ computed over the four sessions, respectively.

The inconsistency scores for all participants as well as their box plot are shown in Fig. 4. In most cases (i.e., $N = 5, 10, 15$, and 25), the GMM yielded substantially more consistent results (i.e., smaller inconsistency scores) than the HMM ($N = 5$: Cohen's $d = 1.16, t_{1002} = -29.5, p < 10^{-137}$; $N = 10$: $d = 0.80, t_{1002} = -30.2, p < 10^{-141}$; $N = 15$: $d = 1.18, t_{1002} = -35.3, p < 10^{-177}$; $N = 25$: $d = 1.27, t_{1002} = -37.0, p < 10^{-189}$ in two-sample t -tests). For $N = 50$, we did not find a substantial difference in the two groups although the difference was statistically significant due to a large sample size ($d = 0.142, t_{1002} = 4.83$, and $p < 10^{-5}$). The results indicate that the HMM does not always outperform the GMM.

IV. DISCUSSION

We carried out a comparative analysis of the GMM and HMM with two components using synthesized and empirical fMRI data. In one type of synthetic state-transition dynamics with which the hidden state does not obey a Markov chain but obeys a deterministic dynamics, the HMM underperformed or at most performed similarly to the GMM in terms of the accuracy of estimating the hidden state (Figs. 3(b) and 3(e)). Furthermore, for the fMRI data with relatively small dimensions, N (i.e., $N \leq 25$), the participant-dependent frequency of the hidden state was often more similar across sessions when the hidden states were estimated by the GMM than by the HMM (Fig. 4). We consider that the HMMs have performed relatively poorly because the state transition dynamics with these synthetic and empirical data considerably deviate from Markovian dynamics (Table I and Fig. 2). In fact, the HMM also underperformed the GMM when the state-transition dynamics were completely memoryless, which is a special case of being Markovian (Figs. 3(a) and 3(d)). This result is probably because a simple model is in general better when the given data do not have complex structure [49].

The validity of using HMMs could be influenced by the sampling rate of the data. If sampling is frequent and the actual brain dynamics have a higher-order temporal structure on the time scale of the sampling period, the state-transition dynamics of the data may considerably deviate from the first order dynamics (i.e., Markovian process), which HMMs assume. In contrast, if one samples the data sparsely enough, then temporal relationships between three consecutive samples (i.e., second-order Markovian process) or more would be eliminated such that the sampled time series possesses up to first order dependency. However, the number of samples thus obtained may be too small to allow us to reliably infer the parameters of an HMM. In practice, HMMs are efficient with a reasonable sampling rate with which the contribution of the first-order dynamics dominates [50]. There is no guarantee that the sampling rate with which the discrete-time dynamics are approximately of first order matches the time scale of neural dynamics of biological interest.

When the given data are short, GMMs are probably more advantageous than HMMs in that a GMM with the same number of components as an HMM is better at avoiding overfitting. Furthermore, GMMs seem to be also advantageous over HMMs when the given data are long or the estimation procedure has to be run many times. Up to our numerical effort, estimation of GMMs was at least a couple of times faster than that of HMMs including when we attempted to estimate models with more than two states. This observation is consistent with a previous study reporting that

estimation of the HMM is often computationally challenging when the data is long or the number of participants is large [18]. It should be noted that, even if a GMM outperforms an HMM, we are not claiming that actual brain dynamics should be regarded to be memoryless. Rather, because the GMM does not impose a particular assumption on state-transition dynamics such as the Markovian property, the GMM is more versatile in describing state-transition dynamics, such as deterministic ones, than the HMM. These advantages of GMMs over HMMs may contribute to the understanding of brain function. If one fits a GMM to fMRI data separately for individual participants, a more accurate characterization of the brain state dynamics than that achieved by existing group level analyses [10, 14, 20, 21, 23] may be realized. If this is the case, dynamics of the brain state may be found to be associated with, wakefulness and sleep [51], attention-deficit/hyperactivity disorder (ADHD) [52], and schizophrenia [27], to name a few.

We refrained from optimizing the number of hidden states. This is because there is no established way to do so from data [53, 54], although some methods based on, e.g., the free energy in the VB algorithms [37] and the number of appearance of each state in the estimated hidden-state time courses [17], have practically been used. In previous studies using fMRI data, the estimated numbers of hidden states are distributed in a wide range, i.e., between 5 and 19 [11, 14, 18, 27, 51, 52]. In contrast to these studies, we assumed two hidden states for the sake of simplicity. This choice was also motivated by a previous study reporting that the hidden states were robustly agglomerated into two clusters in human fMRI data and that the frequency of the two states was heritable and related to cognitive measures [17]. We also found in our previous work with energy landscape analysis that transitions among two or three macroscopic states were correlated with participants' behavior in a bistable visual perception task [21] and executive function [24]. Therefore, we believe that characterizing brain dynamics by transitions among an *a priori* determined small number of states, as we have done in the present study, is a useful approach.

To summarize, we suggest the use of GMMs in situations where HMMs are a standard choice, unless the ground truth about the state transition is supposed to be first-order Markovian. With GMMs, we still retain capability of analyzing dynamics of hidden states, which one may be able to relate to brain function and dysfunction. The present investigation has not exploited specificity of fMRI signals except that data from each individual are relatively short. Therefore, applying both GMMs and HMMs and comparing the obtained results is expected to be equally a good practice for understanding other types of neural and non-neural time series data.

ACKNOWLEDGMENTS

TE acknowledges the support provided through PRESTO, JST (No. JPMJPR16D2). Data were provided by the Human Connectome Project, WU-Minn Consortium (Principal Investigators: David Van Essen and Kamil Ugurbil; 1U54MH091657) funded by the 16 NIH Institutes and Centers that support the NIH Blueprint for Neuroscience Research; and by the McDonnell Center for Systems Neuroscience at Washington University.

REFERENCES

- [1] Raichle ME, et al. (2001) A default mode of brain function. *Proc. Natl. Acad. Sci. USA* 98:676–682.
- [2] Fox MD, et al. (2005) The human brain is intrinsically organized into dynamic, anticorrelated functional networks. *Proc. Natl. Acad. Sci. USA* 102:9673–9678.
- [3] Sporns O (2011) *Networks of the Brain* (MIT Press, Cambridge).
- [4] Deco G, Tononi G, Boly M, Kringelbach ML (2015) Rethinking segregation and integration: contributions of whole-brain modelling. *Nat. Rev. Neurosci.* 16:430–439.
- [5] Tononi G, Edelman GM, Sporns O (1998) Complexity and coherency: integrating information in the brain. *Trends Cogn. Sci.* 2:474–484.
- [6] Bressler SL, Menon V (2010) Large-scale brain networks in cognition: emerging methods and principles. *Trends Cogn. Sci.* 14:277–290.
- [7] Menon V (2011) Large-scale brain networks and psychopathology: a unifying triple network model. *Trends Cogn. Sci.* 15:483–506.
- [8] Calhoun VD, Adali T (2012) Multisubject independent component analysis of fMRI: a decade of intrinsic networks, default mode, and neurodiagnostic discovery. *IEEE Rev. Biomed. Eng.* 5:60–73.
- [9] Bassett DS, Sporns O (2017) Network neuroscience. *Nat. Neurosci.* 20:253–364.
- [10] Baker AP, et al. (2014) Fast transient networks in spontaneous human brain activity. *eLife* 2014:3:e01867.
- [11] Ryali S, et al. (2016) Temporal dynamics and developmental maturation of salience, default and central-executive network interactions revealed by variational Bayes hidden Markov modeling. *PLOS Comput. Biol.* 12:e1005138.

- [12] Vidaurre D, et al. (2016) Spectrally resolved fast transient brain states in electrophysiological data. *Neuroimage* 126:81–95.
- [13] Taghia J, et al. (2017) Bayesian switching factor analysis for estimating time-varying functional connectivity in fMRI. *Neuroimage* 155:271–290.
- [14] Vidaurre D, Smith SM, Woolrich MW (2017) Brain network dynamics are hierarchically organized in time. *Proc. Natl. Acad. Sci. USA* 114:12827–12832.
- [15] Warnick R, et al. (2018) A Bayesian approach for estimating dynamic functional network connectivity in fMRI data. *J. Am. Stat. Assoc.* 113:134–151.
- [16] Brookes MJ, et al. (2018) Altered temporal stability in dynamic neural networks underlies connectivity changes in neurodevelopment. *Neuroimage* 174:563–575.
- [17] Vidaurre D, et al. (2018) Spontaneous cortical activity transiently organises into frequency specific phase-coupling networks. *Nat. Commun.* 9:2987.
- [18] Vidaurre D, et al. (2018) Discovering dynamic brain networks from big data in rest and task. *Neuroimage* 180:646–656.
- [19] Allen EA, et al. (2014) Tracking whole-brain connectivity dynamics in the resting state. *Cereb. Cortex* 24:663–676.
- [20] Calhoun VD, Miller R, Pearlson G, Adali T (2014) The chronnectome: time-varying connectivity networks as the next frontier in fMRI data discovery. *Neuron* 84:262–274.
- [21] Watanabe T, Masuda N, Megumi F, Kanai R, Rees G (2014) Energy landscape and dynamics of brain activity during human bistable perception. *Nat. Commun.* 5:4765.
- [22] Watanabe T, et al. (2014) Energy landscapes of resting-state brain networks. *Front. Neuroinform.* 8:12.
- [23] Ezaki T, Watanabe T, Ohzeki M, Masuda N (2017) Energy landscape analysis of neuroimaging data. *Phil. Trans. R. Soc. A* 375:20160287.
- [24] Ezaki T, Sakaki M, Watanabe T, Masuda N (2018) Age-related changes in the ease of dynamical transitions in human brain activity. *Hum. Brain Mapp.* 39:2673–2688.
- [25] Taghia J, et al. (2018) Uncovering hidden brain state dynamics that regulate performance and decision-making during cognition. *Nat. Commun.* 9:2505.
- [26] Watanabe T, Rees G (2017) Brain network dynamics in high-functioning individuals with autism. *Nat. Commun.* 8:16048.

- [27] Kottaram A, et al. (2019) Brain network dynamics in schizophrenia: reduced dynamism of the default mode network. *Hum. Brain Mapp.* 40:2212–2228.
- [28] Everitt BS, Bullmore ET (1999) Mixture model mapping of brain activation in functional magnetic resonance images. *Hum. Brain Mapp.* 7:1–14.
- [29] Hartvig NV, Jensen JL (2000) Spatial mixture modeling of fMRI data. *Hum. Brain Mapp.* 11:233–248.
- [30] Górriz JM, et al. (2009) Automatic selection of ROIs in functional imaging using Gaussian mixture models. *Neurosci. Lett.* 460:108–111.
- [31] Dempster AP, Laird NM, Rubin DB (1977) Maximum likelihood from incomplete data via the EM algorithm. *J. Royal Stat. Soc. B* 39:1–22.
- [32] Lindsay BG (1995) Mixture models: theory, geometry and applications. In *NSF-CBMS Regional Conference Series in Probability and Statistics* (Institute of Mathematical Statistics, Hayward).
- [33] Pedregosa F, et al. (2011) Scikit-learn: machine learning in Python. *J. Mach. Learn. Res.* 12:2825–2830.
- [34] Ephraim Y, Merhav N (2002) Hidden Markov processes. *IEEE Trans. Inf. Theory* 48:1518–1569.
- [35] Baum LE, Petrie T, Soules G, Weiss N (1970) A maximization technique occurring in the statistical analysis of probabilistic functions of Markov chains. *Ann. Math. Stat.* 41:164–171.
- [36] Viterbi AJ (1967) Error bounds for convolutional codes and an asymptotically optimum decoding algorithm. *IEEE Trans. Inf. Theory* 13:260–269.
- [37] Rezek I, Roberts S (2005) Ensemble hidden Markov models with extended observation densities for biosignal analysis. In *Probabilistic Modeling in Bioinformatics and Medical Informatics* (Springer-Verlag, London). pp 419–450.
- [38] Schölvinck ML, Maier A, Ye FQ, Duyn JH, Leopold DA (2010) Neural basis of global resting-state fMRI activity. *Proc. Natl. Acad. Sci. USA* 107:10238–10243.
- [39] Murphy K, Fox MD (2017) Towards a consensus regarding global signal regression for resting state functional connectivity MRI. *Neuroimage* 154:169–173.
- [40] Van Essen DC, et al. (2012) The human connectome project: a data acquisition perspective. *Neuroimage* 62:2222–2231.
- [41] Smith SM, et al. (2013) Resting-state fMRI in the human connectome project. *Neuroimage* 80:144–168.
- [42] Salimi-Khorshidi G, et al. (2014) Automatic denoising of functional MRI data: combining independent component analysis and hierarchical fusion of classifiers. *Neuroimage* 90:449–468.

- [43] Griffanti L, et al. (2014) ICA-based artefact removal and accelerated fMRI acquisition for improved resting state network imaging. *Neuroimage* 95:232–247.
- [44] Robinson EC, et al. (2014) MSM: a new flexible framework for multimodal surface matching. *Neuroimage* 100:414–426.
- [45] Glasser MF, et al. (2016) A multi-modal parcellation of human cerebral cortex. *Nature* 536:171–178.
- [46] Smith SM, Hyvärinen A, Varoquaux G, Miller KL, Beckmann CF (2014) Group-PCA for very large fMRI datasets. *Neuroimage* 101:738–749.
- [47] Hyvärinen A (1999) Fast and robust fixed-point algorithms for independent component analysis. *IEEE Trans. Neural Netw.* 10:626–634.
- [48] Beckmann C, Smith S (2004) Probabilistic independent component analysis for functional magnetic resonance imaging. *IEEE Trans. Med. Imag.* 23:137–152.
- [49] Bishop CM (2006) *Pattern recognition and machine learning* (Springer, New York).
- [50] Martinez-Diaz M, Fierrez J, Freire M R, Ortega-Garcia J (2007) On the effects of sampling rate and interpolation in HMM-based dynamic signature verification. In *Ninth International Conference on Document Analysis and Recognition*. pp. 1113–1117.
- [51] Stevner AB, et al. (2019) Discovery of key whole-brain transitions and dynamics during human wakefulness and non-REM sleep. *Nat. Commun.* 10:1035.
- [52] Scofield JE, Johnson JD, Wood PK, Geary DC (2019) Latent resting-state network dynamics in boys and girls with attention-deficit/hyperactivity disorder. *PLOS ONE* 14:e0218891.
- [53] Pohle J, Langrock R, van Beest FM, Schmidt NM (2017) Selecting the number of states in hidden Markov models: pragmatic solutions illustrated using animal movement. *J. Agr. Biol. Envi. St.* 22:270–293.
- [54] Celeux G, Durand JB (2008) Selecting hidden Markov model state number with cross-validated likelihood. *Comput. Stat.* 23:541–564.

	<i>From state 1 to 2</i>			<i>From state 2 to 1</i>		
	<i>Empirical</i>	<i>HMM</i>	<i>HMM/Emp.</i>	<i>Empirical</i>	<i>HMM</i>	<i>HMM/Emp.</i>
$N = 5$	0.0446	0.0539	1.21	0.0521	0.0619	1.19
$N = 10$	0.0450	0.0532	1.18	0.0448	0.0536	1.19
$N = 15$	0.0494	0.0586	1.19	0.0460	0.0552	1.20
$N = 25$	0.0427	0.0530	1.24	0.0475	0.0584	1.23
$N = 50$	0.0409	0.0518	1.27	0.0330	0.0443	1.34

TABLE I. Comparison between the empirical state-transition probabilities computed from the estimated time courses of the hidden state (labeled “Empirical”) and those expected from the estimated HMM (labeled “HMM”).

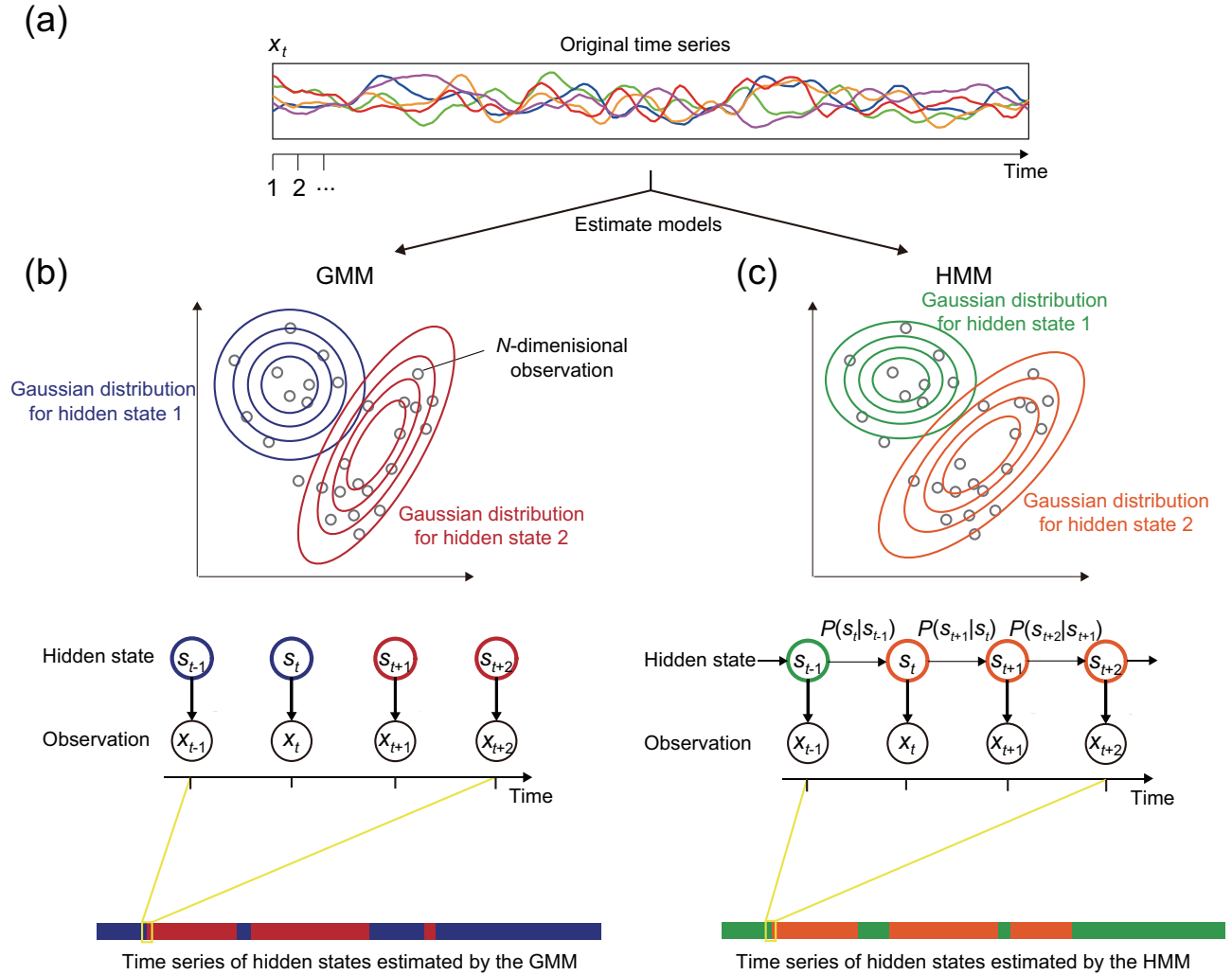


FIG. 1. Overview of the estimation of hidden-state dynamics using GMMs and HMMs. (a) A multivariate time series in discrete time such as fMRI data. (b) One fits a GMM with two components to the multivariate time series data shown in (a). The case of $N = 2$ is schematically shown. The estimation of the GMM enables us to associate one of the hidden states (shown in color) to the data point at each discrete time, x_t . Using the estimated GMM, one can estimate the time course of the hidden state. (c) One fits an HMM with two hidden states to the same data. In general, how the data points are clustered into two hidden states is different between the GMM and HMM. Using the estimated HMM, one can estimate the time course of the hidden state.

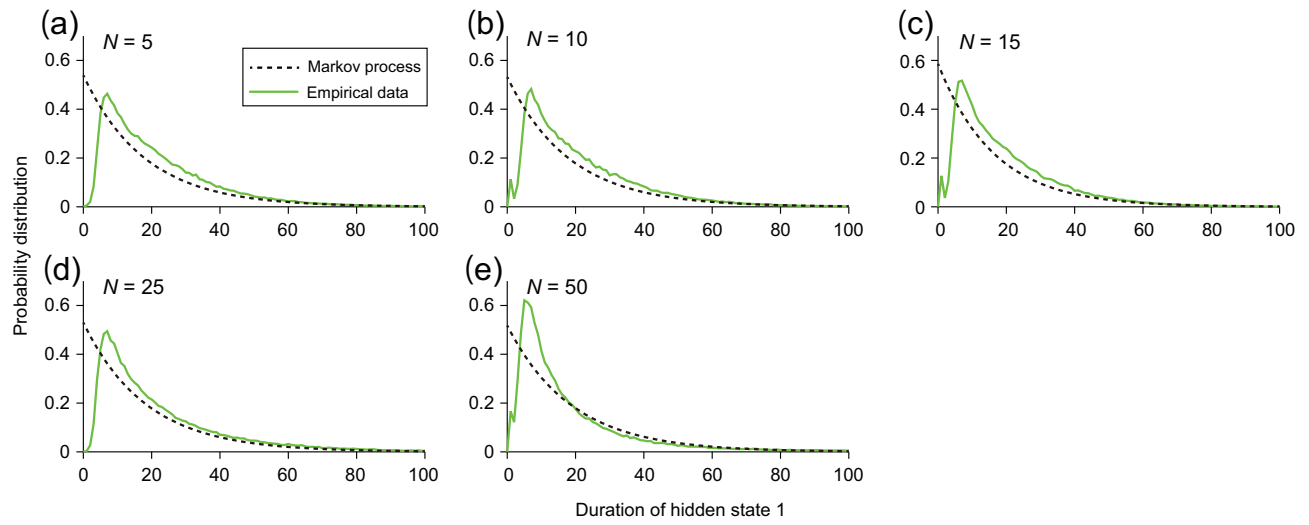


FIG. 2. Distribution of the duration of hidden state 1. The solid lines represent the distribution for the fMRI data, where the dynamics of the hidden state are estimated by the HMM. The dashed lines represent the geometric distribution that the estimated HMM theoretically produces.

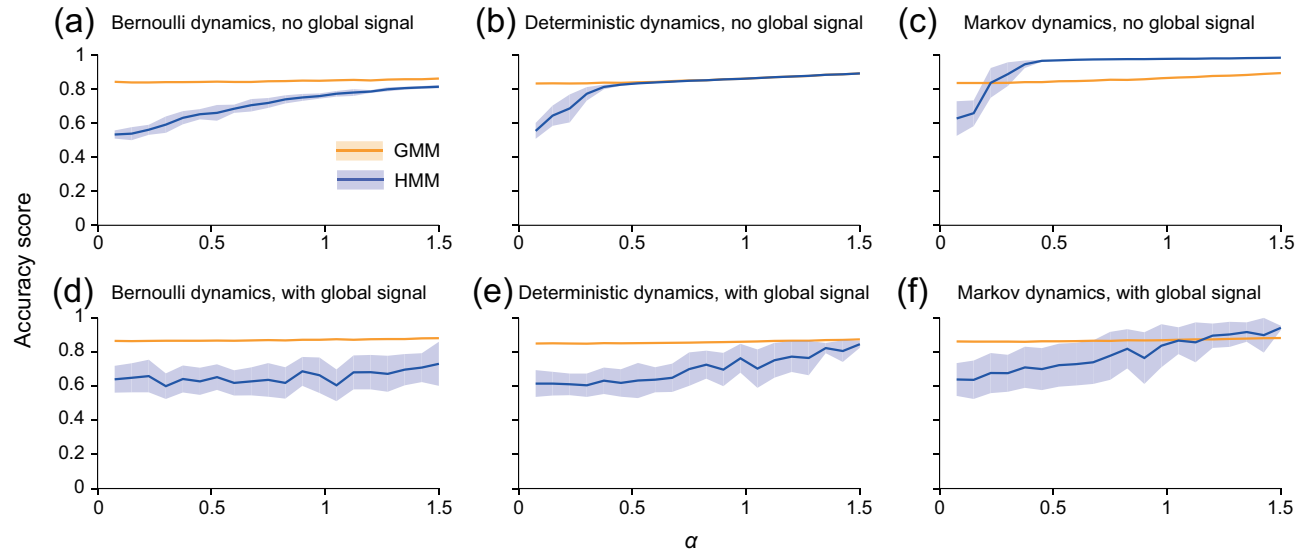


FIG. 3. Accuracy of estimating the hidden states of synthetic data. (a) Synthetic data without the global signal, Bernoulli state dynamics. (b) Without the global signal, deterministic state dynamics. (c) Without the global signal, Markov state dynamics. (d) With the global signal, Bernoulli state dynamics. (e) With the global signal, deterministic state dynamics. (f) With the global signal, Markov state dynamics. The shaded regions represent one standard deviation.

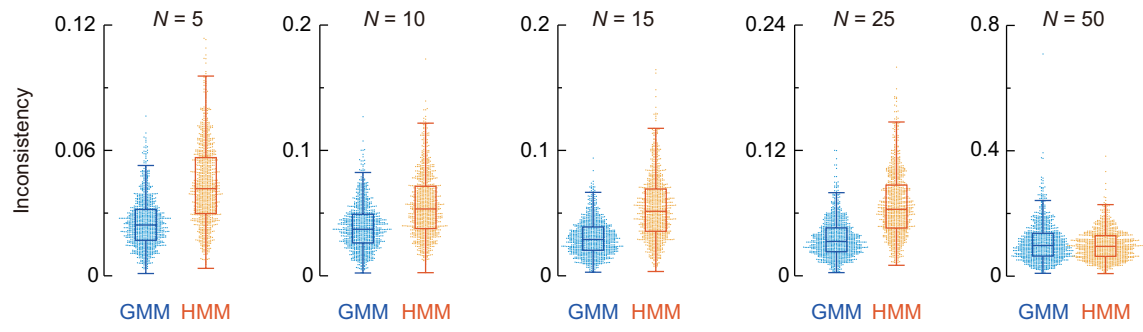


FIG. 4. Reproducibility in terms of the frequency of hidden state 1 in the fMRI data. Each dot represents the inconsistency for a participant. The whiskers of each box plot represent the maximum and minimum values after excluding outliers. The boxes represent the range between the first and third quartile values, and the median of the data.

SUPPORTING INFORMATION

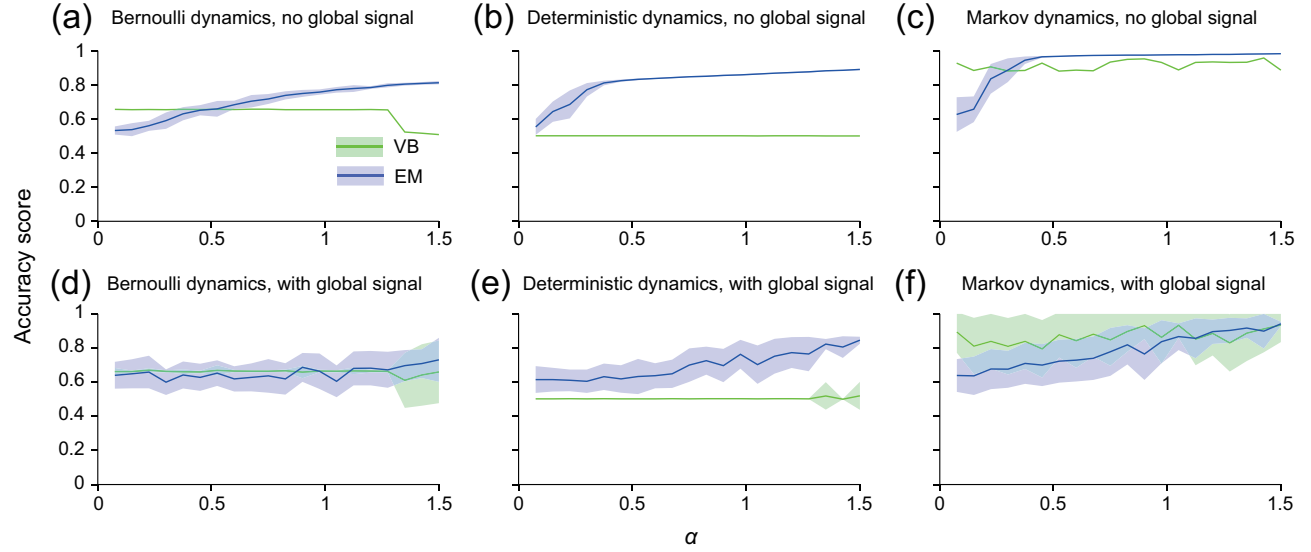


FIG. S1. Comparison between expectation-maximization (EM) and variational-Bayes (VB) algorithms. The accuracy of the estimated hidden states for the synthetic data is shown. (a) Synthetic data without the global signal, Bernoulli state dynamics. (b) Without the global signal, deterministic state dynamics. (c) Without the global signal, Markov state dynamics. (d) With the global signal, Bernoulli state dynamics. (e) With the global signal, deterministic state dynamics. (f) With the global signal, Markov state dynamics. The shaded regions represent one standard deviation.